A&A, 710, A259 (2026)
https://doi.org/10.1051/0004-6361/202659962

Astronomy & Astrophysics

Temporal evolution of the circumstellar disc orientation in the transient X-ray pulsar GRO J1008−57

Yongfeng Hu[1,⋆], Hua Xiao[1], Sergey S. Tsygankov[1,2,3], Long Ji[4], Juri Poutanen[1], and Runting Huang[5]

[1] Department of Physics and Astronomy, FI-20014 University of Turku, Finland
[2] Institut für Astronomie und Astrophysik, Universität Tübingen, Sand 1, D-72076 Tübingen, Germany
[3] Key Laboratory of Particle Astrophysics, Institute of High Energy Physics, Chinese Academy of Sciences, Beijing 100049, China
[4] School of Physics and Astronomy, Sun Yat-sen University, Zhuhai 519082, People's Republic of China
[5] Independent Researcher, Guangdong, People's Republic of China

Received 20 March 2026 / Accepted 15 May 2026

ABSTRACT

The transient X-ray pulsar GRO J1008−57 was previously found to exhibit Type I outbursts occurring at stable orbital phases before its first observed Type II outburst in 2012. We extend the study to investigate the phase evolution after several Type II outbursts using long-term Swift/BAT and MAXI/GSC observations. Our results reveal that the orbital phases of Type I outbursts follow a step-like evolution: they remain largely stable over many orbital periods, but undergo abrupt small-amplitude jumps coincident with each Type II outburst. This step-like behaviour is difficult to explain with the commonly proposed mechanisms involving a highly eccentric or precessing disc around a Be star. The energetics of Type I X-ray outbursts shows a systematic increase before Type II outbursts, followed by a rapid decline and a subsequent gradual recovery. This behaviour suggests cycles of disc depletion and reconstruction driven by Type II outbursts. Considering the small amplitude of each phase jumps, we propose that this step-like phase evolution might be related to the long orbital period of GRO J1008−57, implying infrequent neutron star–disc interactions. After disc depletion by Type II outbursts, the disc around the Be star has enough time to rebuild its density and restore a geometric structure similar to its pre–Type II outburst state. Consequently, the orbital phases of subsequent Type I outbursts not only change very slightly, but can also remain stable over many orbital periods until the next Type II-driven disc reconfiguration, yielding the observed step-like evolution.

Key words. accretion, accretion disks – pulsars: general

1. Introduction

Be/X-ray binaries (BeXRBs) are a common type of high-mass X-ray binaries (HMXB) that contain a compact object (typically a neutron star) and a main-sequence O/B star (see Reig 2011 for a review). The Be designation of the O/B star originates from the characteristic Balmer-series emission lines observed in its optical spectrum. It also exhibits an infrared excess relative to normal O/B stars (Porter & Rivinius 2003; Rivinius 2019). These two observational properties are interpreted as clear indicators of a geometrically thin circumstellar decretion disc that surrounds the Be star (Porter & Rivinius 2003). This disc is thought to be formed by the high-speed rotation of the Be star that triggers the outflow of material from its equatorial plane, which then undergoes viscous diffusion into a Keplerian disc (Lee et al. 1991). When the decretion disc expands beyond the Roche lobe, the neutron star can capture and accrete material from the disc.

The accreted matter is channelled along the magnetic field onto the magnetic poles of the neutron star, ultimately converting the gravitational energy of the accreting material into X-rays (see e.g. Mushtukov & Tsygankov 2024). Most BeXRBs are X-ray transients, and their behaviour is characterised by two types of outbursting activity (Negueruela et al. 1998). Type I X-ray outbursts (normal outbursts), which last for only a small fraction of the orbital period in long-period systems, are periodic in nature and are often observed at the periastron passage with a typical luminosity of $L_x \sim 10^{36}$–10^{37} erg s^{-1}. Type II X-ray outbursts (giant outbursts) occur much less frequently, but have a higher luminosity of $L_x > 10^{37}$ erg s^{-1} and last for a large fraction of an orbital period or even for several orbital periods, showing no preferred orbital phase (Reig 2011; Martin et al. 2014a; Okazaki & Negueruela 2001). Type I outbursts are commonly interpreted to be the result of interactions that occur when the neutron star makes its closest approach to the circumstellar disc of the Be star in each orbital cycle (Okazaki & Negueruela 2001; Okazaki et al. 2013). Type II outbursts are thought to be related to a highly misaligned and increasingly eccentric decretion disc, which causes a prolonged interaction with the neutron star (Okazaki et al. 2013; Martin et al. 2014a; Monageng et al. 2017).

However, from actual observations, it has been discovered that the orbital phase of Type I outbursts does not always coincide with the periastron, and the outbursts may occur either before or after the periastron. Moreover, during Type II outbursts, the phase of Type I outbursts may suddenly shift with the following gradual recovery over several hundred days. Sometimes, the orbital phases of Type I outbursts exhibit a periodic alternation between phase delays and phase advances. Detailed studies of the orbital phase variations of Type I outbursts in EXO 2030+375 have been reported by Wilson et al. (2002, 2005, 2008), Baykal et al. (2008), Laplace et al. (2017), and Huang et al. (2025), providing a representative example.

It should be emphasised thatType I and Type II outbursts both essentially originate from the interaction between the neutron star and the Be disc. Consequently, these puzzling orbital phase

⋆ Corresponding author: yongfeng.hu@utu.fi

variations reflect the structure, the physical properties, and temporal evolution of the Be disc, which sometimes changes continuously. Although some theoretical models have described these changes, the actual physical interaction between a neutron star and a Be disc remains difficult to study. Nevertheless, it is essential to study these phase variations in a larger sample of sources from a phenomenological and physical point of view, and it provides key input for refining current theoretical models. However, this requires observations of sources that exhibit multiple and regular outbursts, and one of the most promising candidates for such a study is GRO J1008−57.

The BeXRB GRO J1008−57 is composed of a transient X-ray pulsar with a spin period of 93.5 s (Stollberg et al. 1993) and a B0e star at a distance of 3.6 kpc (Fortin et al. 2022). The orbit of the binary has a period of 249.48 d and an eccentricity of 0.68 (Coe et al. 2007; Kühnel et al. 2013). Since its discovery by the *Compton Gamma Ray Observatory* (*CGRO*) during the 1993 X-ray outburst (Stollberg et al. 1993; Wilson et al. 1994), it exhibited periodic Type I outbursts around the periastron passage over many years. Previously, Kühnel et al. (2013) reported that the orbital phase of Type I outbursts in GRO J1008−57 was remarkably stable between 2005 and 2012, before it exhibited the first Type II outburst. However, since the works by Kühnel et al. (2013), GRO J1008−57 has experienced a total of four Type II outbursts, which were detected in November 2012 (Kuehnel et al. 2012), January 2015 (Kretschmar et al. 2015), August 2017 (Sguera 2017), and June 2020 (Nakajima et al. 2020; Wang et al. 2021). Based on these findings, therefore, GRO J1008−57 is an ideal object for studying the orbital phase evolution of Type I and Type II outbursts. We investigate the orbital phase evolution of Type I outbursts after several Type II outbursts in GRO J1008−57 and compare it with previous studies. The paper is organised as follows. Section 2 briefly describes the observations. The data analysis and results are given in Sect. 3. Finally, we discuss the results and present the conclusions in Sect. 4.

2. Observations

The Burst Alert Telescope (BAT) is one of three instruments on board the *Neil Gehrels Swift Observatory* (*Swift*; Gehrels et al. 2004) spacecraft designed to study gamma-ray bursts. Operating in the 15–150 keV energy range, the BAT provides an energy resolution of ∼7 keV, a sensitivity of $\sim 10^{-8}$ erg s^{-1} cm^{-2}, and a field of view of 1.4 sr. It performs an all-sky hard X-ray survey with a sensitivity of ∼2 mCrab (systematic limit), while serving as a monitor for hard X-ray transients (Gehrels et al. 2004; Barthelmy et al. 2005). In order to estimate the flux variability during outbursts, we used daily light curves of GRO J1008−57 provided by the website of the Swift/BAT Hard X-ray Transient Monitor[1].

The Monitor of All-sky X-ray Image (MAXI; 2–30 keV) is mounted at the International Space Station. Its scientific instruments consist of two types of X-ray cameras with a wide field of view: the Solid-state Slit Camera (SSC), and the Gas Slit Camera (GSC). The main role of the GSC is to serve as the X-ray all-sky monitor (Matsuoka et al. 2009). We also tracked the outburst activity of GRO J1008−57 in the soft X-ray band using data from the MAXI/GSC website[2].

[1] https://swift.gsfc.nasa.gov/results/transients/GROJ1008-57/

[2] https://maxi.riken.jp/star_data/J1009-582/J1009-582.html

To study the total energy release during Type I outbursts, the Swift/BAT and MAXI/GSC count rates were converted into energy fluxes assuming the Crab nebula as a standard candle. We adopted a conversion of 1 Crab = 0.22 count s^{-1} cm^{-2} = 1.4×10^{-8} erg cm^{-2} s^{-1} for the BAT data in the 15–50 keV band (Krimm et al. 2013) and 1 Crab = 3.6 count s^{-1} cm^{-2} = 3.1×10^{-8} erg cm^{-2} s^{-1} for the MAXI data in the 2–20 keV band (Matsuoka et al. 2009). The count rates were converted into energy fluxes and used to estimate the total radiated energy during each outburst, assuming a source distance of 3.6 kpc.

3. Data analysis and results

3.1. Light curve

Figure 1 shows the light curve of GRO J1008−57 as observed by *Swift*/BAT and MAXI/GSC, revealing regular and stable luminosity variations in the source over long timescales. Since Type I outbursts are generally thought to occur near periastron passage, we calculated the times of periastron passage for each orbital period using the ephemeris from Kühnel et al. (2013), which provides an orbital period of P = 249.48 d and a periastron time of MJD 54424.71. A total of 31 and 24 Type I outbursts can be identified in the *Swift*/BAT and MAXI/GSC observations, respectively. In our numbering convention, the epoch of the Type I outburst number n can be expressed as its periastron time T_n = MJD 53426.789 + n×249.48, where n is the number of orbits since the outburst in 2005. In addition, the positions of four Type II outbursts are marked with grey shaded regions, allowing us to specifically examine the phase variations of Type I outbursts occurring in their vicinity.

3.2. The start and peak times of Type I outbursts

In order to determine when Type I outbursts occurred during each orbital period, we modelled the temporal profiles of Type I outbursts in GRO J1008−57 using a simplified fast-rise exponential-decay (FRED) function (e.g. Rikame et al. 2025), comprising a linear rise, an exponential decay, and constant background component, as given by

$$F_{\text{burst}}(t) = \begin{cases} C_1, & \text{if } t < t_{\text{start}}, \\ A \dfrac{t - t_{\text{start}}}{t_{\text{peak}} - t_{\text{start}}} + C_1, & \text{if } t_{\text{start}} \leq t < t_{\text{peak}}, \\ C_2 + (A + C_1 - C_2)\, e^{-\frac{t - t_{\text{peak}}}{\tau}}, & \text{if } t \geq t_{\text{peak}}, \end{cases} \quad (1)$$

where t is the time, t_{start} and t_{peak} denote the start and peak times of the outburst, A is the outburst amplitude, τ is the exponential decay timescale, and the constants C_1 and C_2 represent the local persistent emission levels before and after the peak of the outburst, respectively. This model enabled us to simultaneously fit and estimate the onset and peak times of all Type I outbursts in GRO J1008−57[3]. Outbursts #1 and #29 (*Swift*) and outburst #31 (MAXI), which have significant data gaps (Fig. 4), were excluded from our sample. The fitting time interval for each orbital period was set within ±0.5 orbital periods around the periastron passage, and the uncertainties of the fitted start and peak times were estimated from the covariance matrix of the fit. They correspond to 1σ confidence intervals.

[3] We also applied the Gaussian model adopted by Laplace et al. (2017) and Huang et al. (2025) to determine the peak times, and we obtained results similar to those derived from the FRED model.

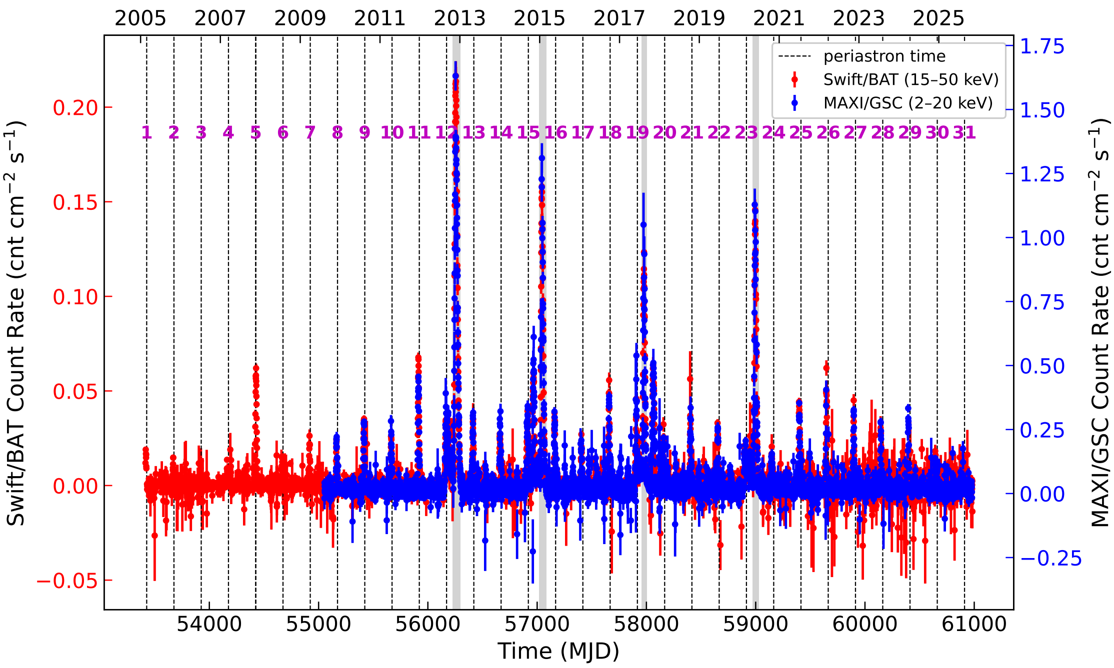

Fig. 1. Long-term light curves of GRO J1008−57 obtained with *Swift*/BAT (15–50 keV; red points) and MAXI/GSC (2–20 keV; blue points). The shaded regions indicate the four Type II outbursts occurring in 2012, 2015, 2017, and 2020. The vertical dashed lines indicate the periastron times of each orbital period, calculated using the ephemeris from Kühnel et al. (2013). The purple numbers represent the 31 Type I outbursts detected by *Swift*/BAT and the 24 detected by MAXI/GSC. The profiles of all Type I outbursts are shown in Fig. 4.

After obtaining the best-fit timing results using the FRED model, we calculated the orbital phases of the onset and peak times of all Type I outbursts by computing their time differences relative to the corresponding periastron passages time, as shown in Fig. 2. The orbital phases of the fitted onset and peak times derived from the two instruments are generally consistent.

Throughout the entire observational history of GRO J1008−57, the orbital phases of the onset and peak times for almost all bursts are consistently and periodically clustered in the vicinity of periastron, more specifically, prior to the periastron passage. However, Type I outbursts occurring close to the four Type II outbursts in 2012, 2015, 2017, and 2020 exhibit more complex behaviours, as illustrated by the detailed light-curve profiles shown in Fig. 3. Near the 2012 and 2020 Type II outbursts, the profiles of bursts #12 and #23 exhibit multi-peaked structures (Fig. 4). In contrast, near the 2015 and 2017 Type II outbursts, bursts #15′ and #20′ are regarded as additional outbursts (see Fig. 3), exhibiting significant abrupt phase shifts relative to periastron. However, the system subsequently returned rapidly to the normal periastron-associated Type I outburst pattern within one orbital period. For the same Type I outburst, the *Swift*/BAT and MAXI/GSC observations not only yield consistent onset and peak times derived from the FRED model fitting, but also show similar light-curve profiles.

3.3. Orbital phase evolution of the Type I outbursts

To further characterise the long-term orbital phase evolution of the Type I outbursts in GRO J1008−57, we present the profiles and corresponding colour-coded intensity map of all Type I outburst light curves observed by *Swift*/BAT and MAXI/GSC in Fig. 4. Most Type I outbursts recur in a stable and periodic pattern close to and typically before periastron phase. Previously, Kühnel et al. (2013) also analysed the orbital phase evolution of Type I outbursts of GRO J1008−57 observed with *Swift*/BAT between 2005 and 2012 (i.e. bursts #1–12; see Fig. 2), all of which occurred before the first observed Type II outburst, and found that no phase evolution was present during this epoch. This also agrees with our results. However, we note that the intensity map of the Type I outbursts here shows that phase shifts begin to appear starting from burst #13, which subsequently followed the first observed Type II outburst in 2012. The most significant phase shift is observed after the fourth Type II outburst in 2020. To quantify this phase shift, we fitted the orbital phase evolution of the onset times of all the Type I outbursts with the linear ($\phi(t) = a + bt$), quadratic ($\phi(t) = a + bt + ct^2$), and step-like model,

$$\phi(t) = \begin{cases} C_1, & t < t_1, \\ C_2, & t_1 \le t < t_2, \\ C_3, & t_2 \le t < t_3, \\ C_4, & t_3 \le t < t_4, \\ C_5, & t \ge t_4, \end{cases} \tag{2}$$

where t is the time, and $t_1 - t_4$ represent the boundary times of the step-like model, which are fixed at the peak times of the four Type II outbursts. Burst 5 (Swift/BAT), which exhibits a significant phase shift and unusually high luminosity (coloured map in Figs. 4 and 6), may represent an intermediate state between Type I and Type II outbursts. We adopted the same treatment as in Kühnel et al. (2013) and excluded this burst from our fitting. The results of the fit are shown in Fig. 5. Then, we applied the Akaike information criterion (AIC=$\chi^2 + 2k + (2k^2 + 2k)/(n - k - 1)$, where χ^2 is the chi-square value, k is the number of free parameters, and n is the number of data points) to choose the best model and found that the step-like model yielded the lowest AIC value compared to the linear and quadratic models for the *Swift*/BAT and MAXI/GSC data. For the onset-phase fits, the ΔAIC values between the step-like model and the linear and quadratic

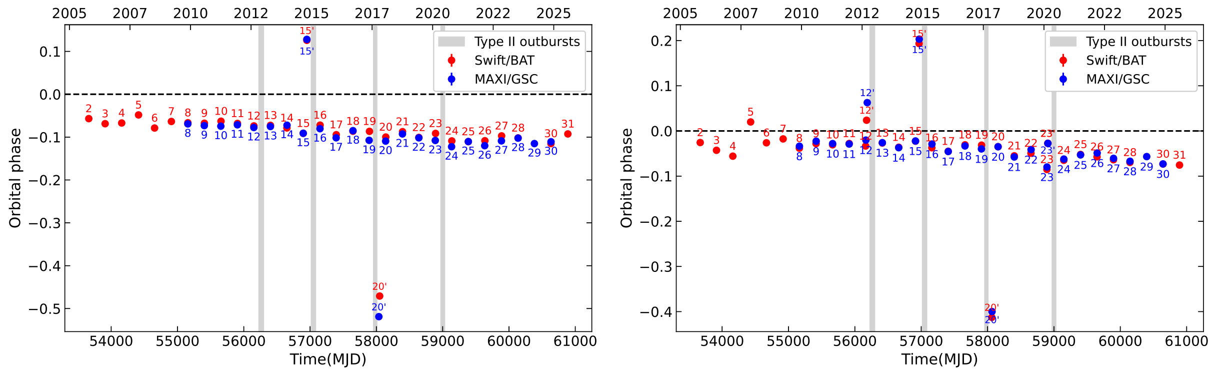

Fig. 2. Left panel: Orbital phases of the onset times of Type I outbursts from GRO J1008−57 observed with *Swift*/BAT (red numbers) and MAXI/GSC (blue numbers). The horizontal dashed line indicates the orbital phase 0, and the shaded vertical regions present the Type II outbursts. Right panel: Same as the left panel, but showing the orbital phases of the peak times of all Type I outbursts.

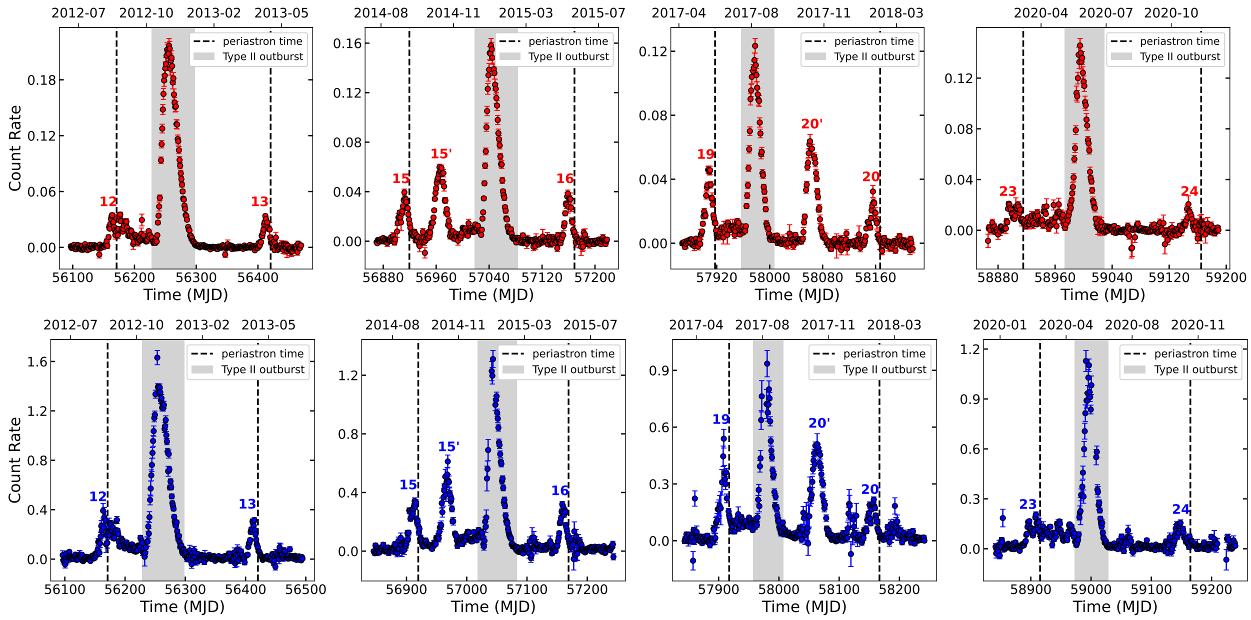

Fig. 3. Light curves of GRO J1008−57 close to the Type II outbursts from the *Swift*/BAT (upper panels) and MAXI/GSC (lower panels) data. The vertical dashed lines present the periastron times, and the shaded regions indicate the Type II outbursts.

Table 1. Step-like model parameters of the evolution of the orbital phase of the onset times of Type I outbursts in GRO J1008−57 from the *Swift*/BAT and MAXI/GSC data.

Step	t_{start}	t_{end}	Avg. phase	$\Delta\phi$	$\Delta\phi/\Delta t$ (d^{-1})
			Swift/BAT		
1	53661	56263	−0.0673 ± 0.0004	–	–
2	56263	57050	−0.0782 ± 0.0008	−0.0108 ± 0.0009	$(-1.38 \pm 0.12) \times 10^{-5}$
3	57050	57982	−0.0832 ± 0.0005	−0.0050 ± 0.0010	$(-5.37 \pm 1.08) \times 10^{-6}$
4	57982	59001	−0.0932 ± 0.0007	−0.0100 ± 0.0009	$(-9.77 \pm 0.85) \times 10^{-6}$
5	59001	60889	−0.1067 ± 0.0008	−0.0136 ± 0.0010	$(-7.18 \pm 0.55) \times 10^{-6}$
			MAXI/GSC		
1	55154	56263	−0.0719 ± 0.0005	–	–
2	56263	57050	−0.0757 ± 0.0009	−0.0038 ± 0.0010	$(-4.87 \pm 1.29) \times 10^{-6}$
3	57050	57982	−0.0844 ± 0.0009	−0.0087 ± 0.0012	$(-9.35 \pm 1.32) \times 10^{-6}$
4	57982	59001	−0.1007 ± 0.0009	−0.0162 ± 0.0012	$(-1.59 \pm 0.12) \times 10^{-5}$
5	59001	60635	−0.1088 ± 0.0006	−0.0081 ± 0.0011	$(-4.96 \pm 0.06) \times 10^{-6}$

Notes. Columns: (1) Step number; (2) t_{start}, start time of the step (MJD); (3) t_{end}, end time of the step (MJD); (4) average orbital phase during the step; (5) $\Delta\phi$, phase change within the step; (6) $\Delta\phi/\Delta t$, average rate of phase evolution, where $\Delta t = t_{end} - t_{start}$.

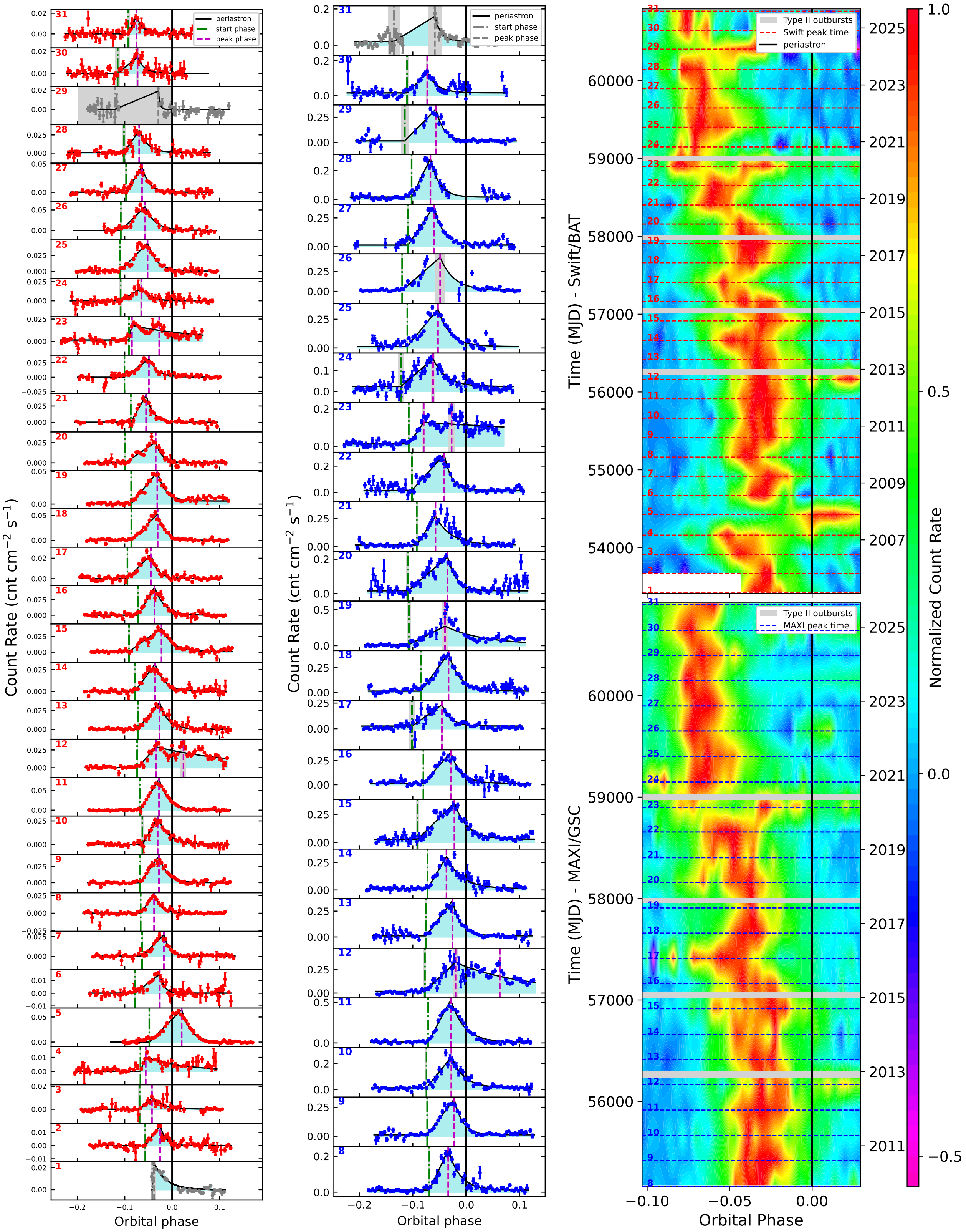

Fig. 4. Evolution of the outburst profiles of GRO J1008−57 . Left panel: Profiles of Type I outbursts observed with *Swift*/BAT, arranged from bottom to top in order of occurrence time. The vertical dashed green and purple lines indicate the burst onset times and peak times, respectively, and the vertical black line marks the periastron at orbital phase 0. Bursts #1, #29 (*Swift*/BAT), and #31 (MAXI/GSC), shown in grey, were excluded from the analysis due to data gaps. The cyan shaded regions used to calculate the total energy released (Fig. 6) during the Type I outbursts indicate that the burst profiles cover a range of ±0.15 orbital period around the peak times. Middle panel: Same as the left panel, but for the profiles of Type I outbursts observed with MAXI/GSC. Right panel: Evolution of the colour-coded intensity profiles of all Type I outbursts observed by *Swift*/BAT and MAXI/GSC, with the peak intensity of each outburst normalised to unity. The horizontal dashed line and numbers indicate the peak times of each Type I outbursts, and the grey shaded regions show the Type II outbursts.

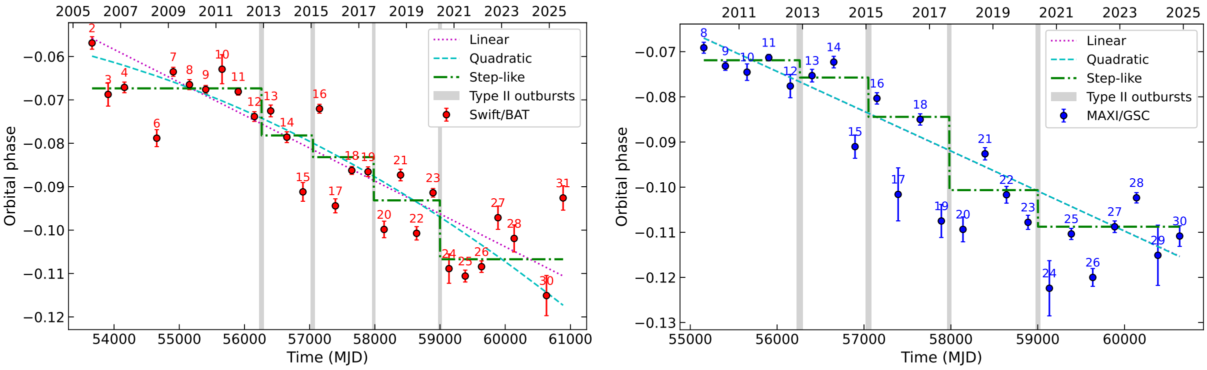

Fig. 5. Evolution of the orbital phase of the onset times of Type I outbursts in GRO J1008−57 using *Swift*/BAT (left panels) and MAXI/GSC (right panels) data and the best-fit models. The shaded vertical regions indicate the Type II outbursts. The dotted, dashed, and dash-dotted purple, cyan, and green lines represent the linear, quadratic, and step-like models, respectively, with the step-like model providing the best fit to both the *Swift*/BAT and MAXI/GSC data. The four step boundaries are fixed at the peak times of the four Type II outbursts.

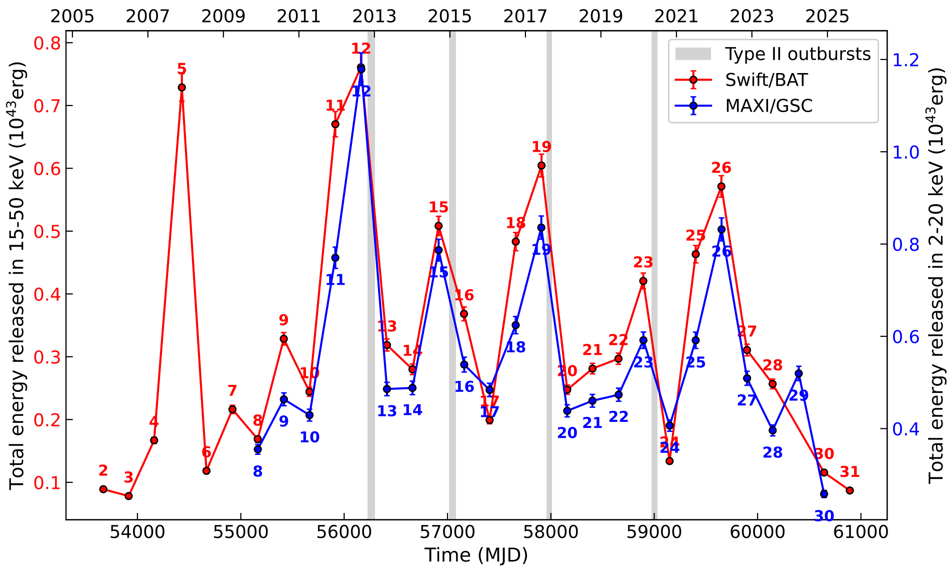

Fig. 6. Evolution of the total energy release of all Type I outbursts in GRO J1008−57, obtained by integrating the fitted model curve over a time interval of ±0.15 orbital period around the burst peak (i.e. the area of the cyan shaded regions in Fig. 4). The red and blue points denote the *Swift*/BAT and MAXI/GSC results, respectively. The shaded regions indicate the Type II outbursts.

models are 76.9 and 37.9 for *Swift*/BAT, and 81.7 and 84.3 for MAXI/GSC, respectively. The corresponding chance improvement probability, calculated as $e^{-\Delta \mathrm{AIC}/2}$ (König et al. 2020), indicates that the significance of the difference between the step-like model and the linear and quadratic models exceeds 5σ. This demonstrates that the step-like model provides the best fit to the orbital phase evolution of the onset times of the Type I outbursts in GRO J1008−57 observed by *Swift*/BAT and MAXI/GSC. These results show that the orbital phase evolution does not follow a continuous long-term gradual drift as described by the linear and quadratic models. Table 1 presents the best-fit results of the step-like model for the *Swift*/BAT and MAXI/GSC. All the phase jumps exhibit relatively small amplitudes. Because the peak phase depends on the outburst morphology (e.g. multi-peaked structures) and duration, we regard it as a less reliable tracer of the neutron star–disc interaction and therefore did not analyse its evolution.

We note that when the X-ray emission in GRO J1008−57 is mediated by an accretion disc, the onset time of Type I outbursts might not directly reflect the instantaneous conditions in the Be circumstellar disc. As discussed by Tsygankov et al. (2017), the source exhibits a moderate X-ray luminosity throughout the entire orbital cycle, which was interpreted in terms of different accretion regimes. As a result, the observed flux increase might occur with some delay associated with the transition of the accretion disc into the hot (ionised) state. Nevertheless, relative shifts in the onset times of Type I outbursts from one orbital cycle to the next can still serve as a tracer of the long-term evolution of the Be disc geometry.

Furthermore, we also investigated the long-term evolution of the total energetics (fluence) of Type I outbursts in GRO J1008−57. The energy released in each outburst was estimated by integrating the fitted model curve over a time interval of ±0.15 orbital phase around the outburst peak (Fig. 6). The burst fluences inferred from *Swift*/BAT and MAXI/GSC data are consistent with each other. Interestingly, in contrast to the orbital phases of Type I outburst onset, which transition between distinct piecewise stable states between Type II outbursts, their total energy release exhibits irregular long-term oscillatory variations. The behaviour of the Type I outburst energetics generally rises before the Type II outburst, followed by a decline afterwards and a subsequent gradual recovery, although the overall picture may be more complicated. A similar rise-and-fall behaviour is also seen in outbursts 5 and 26 (i.e. before the first and after the last Type II outbursts), although they are not associated with Type II outbursts. In addition, the interval after the third Type II outburst (2017–2020) shows a somewhat slower recovery in fluence compared to the other cases.

4. Discussion and conclusion

We investigate the temporal evolution of the orbital phase of Type I outbursts, with particular attention to the effects of several Type II outbursts, using observations from *Swift*/BAT and MAXI/GSC. Our work substantially expands upon the findings of Kühnel et al. (2013), who showed that the orbital phase of Type I outbursts in GRO J1008−57 remained generally stable prior to the first observed Type II outburst in 2012.

In general, our study revealed that the phases of Type I outbursts of GRO J1008−57 follow a step-like evolution, remaining stable over multiple orbital periods and exhibiting abrupt, small amplitude phase jumps (up to −0.0162 in orbital phase; see Table 1) coincident with each Type II outbursts. Each jump presumably occurred over a short timescale (tens of days) because Type II outbursts are relatively short. We note that the orbital period reported by Kühnel et al. (2013) has an uncertainty of ±0.04 d. Over the observed ∼30 orbital cycles, this might accumulate to an uncertainty of ∼1.2 d in the predicted periastron time. However, this value is much lower than the observed total phase shift of ∼0.04 (corresponding to ∼10 d) and therefore cannot explain the observed effect.

However, detailed studies of another transient, Be/XRP EXO 2030+375, revealed distinctly different evolution features. In this system, phase shifts are not only triggered by Type II outbursts, but are sometimes also associated with Type I outbursts (Laplace et al. 2017; Huang et al. 2025). It exhibits a potential 5–10 yr periodicity alternation between positive phase shifts associated with Type II outbursts and negative phase shifts associated with Type I outbursts. Each phase shift showed a large amplitude (up to 0.5 in orbital phase) and was followed by long-term (hundreds of days) phase variations or a gradual recovery towards the periastron phase (Wilson et al. 2002, 2005, 2008; Baykal et al. 2008; Laplace et al. 2017; Huang et al. 2025).

In order to explain the periodic positive and negative phase alternation shifts in EXO 2030+375, Laplace et al. (2017) applied the Kozai-Lidov (KL) framework investigated by Martin et al. (2014b) and Fu et al. (2015a,b), in which a long-term periodic exchange occurs between the eccentricity and inclination of the Be disc. They calculated a KL oscillation timescale of about 10 years for EXO 2030+375, which matches its observed phase alternation shift period above remarkably well.

With the method described in Martin et al. (2014b) and Laplace et al. (2017) and assuming a rigid Be disc of radius R with a surface density profile following a power law, $\Sigma \propto R^{-p}$, we estimate the KL oscillation timescale, $\tau_{\rm KL}$, as

$$\frac{\tau_{\rm KL}}{P_{\rm orb}} \approx \frac{(4-p)}{\left(\frac{5}{2}-p\right)}(1-e)^{-1}\sqrt{\frac{M_{\rm Be}}{M_{\rm NS}}\left(\frac{M_{\rm Be}}{M_{\rm NS}}+1\right)}, \quad (3)$$

where $M_{\rm Be}$ and $M_{\rm NS}$ denote the masses of the Be star and the neutron star, respectively, e is the orbital eccentricity, and $P_{\rm orb}$ is the orbital period of the binary system. For the unknown parameters, we adopted typical values of $p = 1.5$ (Martin et al. 2014b), $M_{\rm Be} = 20\,M_\odot$, and $M_{\rm NS} = 1.4\,M_\odot$ (Okazaki & Negueruela 2001). Using the orbital parameters described in Kühnel et al. (2013), we also estimated a KL oscillation timescale of about 78.9 yr for GRO J1008−57. This timescale exceeds the available observational history of GRO J1008−57 by far, and therefore, the KL-driven mechanism cannot be excluded for the source. On the other hand, this mechanism is expected to produce substantial eccentricity growth and large phase shifts, as observed in EXO 2030+375. These are not seen in GRO J1008−57, however, and the KL-driven phase shifts therefore appear to be questionable.

To explain the long-term phase shift in EXO 2030+375, such as the phase shifts associated with Type I outbursts spanning MJD 50000–50600, Wilson et al. (2002) proposed that these phase shifts were caused by a density perturbation propagating through the Be disc, that is, a global one-armed oscillation, which produces a non-axisymmetric disc and can shift the outburst phase when the neutron star interacts with the perturbed region. This process operates on long timescales, with a characteristic period of 15±3 yr for EXO 2030+375. Density perturbations like this have been inferred from the Hα line profiles observed in Be/X-ray binaries, for instance, 4U 0115+63 (Negueruela & Okazaki 2001; Negueruela et al. 2001), and are thought to operate within individual cycles of disc dispersal or reconstruction. However, for GRO J1008−57, the orbital phases of Type I outbursts exhibit step-like evolutionary features. Except for brief phase jumps occurring at the interval times (tens of days) of the Type II outbursts, the orbital phases remain relatively stable, showing no evidence of a continuous long-term phase drift driven by density perturbations like this. A remarkable stability of Type I outburst phases before the first observed Type II outburst was pointed out by Kühnel et al. (2013). Therefore, this behaviour argues against a global one-armed oscillation-driven phase shift in GRO J1008−57. We note, however, that optical Hα observations of GRO J1008−57 show significant variability in line shape, intensity, and asymmetry (Coe et al. 2007), consistent with a density-perturbed Be disc. Although sparse and predating our X-ray data, these results suggest that global disc perturbations or disc-loss processes may still be present.

Similarly, long-term disc precession (Martin et al. 2014a) is expected to generate prolonged phase recovery towards periastron phase, as observed over ∼500 d in EXO 2030+375 after its 2021 Type II outburst (Huang et al. 2025). In contrast, no comparable long-duration phase recovery is detected in GRO J1008−57 after a Type II outburst, raising questions about the applicability of a precessing Be disc scenario in GRO J1008−57.

In light of the above analysis, the central question therefore is which physical mechanism drives the step-like orbital phase evolution observed in GRO J1008−57. After the mechanisms proposed for EXO 2030+375 were excluded, including the eccentric Be disc driven by KL oscillations, one-armed oscillation, and long-term disc precession, the problem becomes difficult to understand. Independently of the exact nature of the observed properties, it is clear that Type II outbursts play a key role in restructuring the Be disc.

This is further supported by the oscillatory behaviour of the Type I outburst energetics shown in Fig. 6. The systematic increase in energy before Type II outbursts suggests gradual mass accumulation in the Be disc, whereas the rapid decline after Type II outbursts indicates a temporary depletion of the disc material. The subsequent gradual recovery reflects the rebuilding of the disc density and the mass supply. Thus, this fluence evolution is naturally explained within a framework of disc depletion and reconstruction cycles associated with Type II outbursts. Each Type II outburst appears to mark a rapid and different reconfiguration of the disc geometry. However, the causal connection between the disc evolution and Type II outbursts remains uncertain. It is plausible that large-scale perturbations or instabilities in the Be disc lead to Type II outbursts and are not triggered by them. When the Type II outbursts end, the interaction between the neutron star and the Be disc settles into a new temporary configuration, shifting the preferred orbital phase for efficient accretion, and thereby changing the orbital phases of subsequent Type I outbursts.

However, the orbital phases of subsequent Type I outbursts change only slightly and quickly transit into a new stable state, as indicated by the small-amplitude phase jumps in the step-like evolution (see Fig. 5 and Table 1). A likely explanation for this observed difference between EXO 2030+375 and GRO J1008−57 is related to the long orbital period of the latter (249.48 d; Kühnel et al. 2013), which implies a lower frequency of the neutron star–disc interactions. After disc depletion driven by Type II outbursts, the disc has enough time to rebuild its density and restore its geometric structure close to its stable state before Type II outbursts. As a result, the orbital phases of subsequent Type I outbursts not only change very slightly compared to before the Type II outburst, but can ultimately still remain stable phases over many orbital periods until the occurrence of the next Type II–driven disc reconfiguration event. Therefore, these processes can naturally explain the observed step-like phase evolution of GRO J1008−57.

In contrast, EXO 2030+375 has a short orbital period (∼46 d; Wilson et al. 2005), implying more frequent neutron star–disc interactions that can drive large-scale long-term perturbations. As a result, not only Type II outbursts, but also sometimes even typical Type I outbursts can induce significant long-term phase shifts, as observed in 1995 and 2016 (Huang et al. 2025; Laplace et al. 2017; Wilson et al. 2002).

Future multi-wavelength observations will be crucial for further understanding the Be-disc configuration in GRO J1008−57. In particular, optical spectroscopic monitoring of the Hα line profiles can trace the density structure and dynamical evolution of the Be disc, while polarimetric observations may help us to constrain the disc geometry and inclination. Combined with continued X-ray monitoring, these observations will provide a deeper insight into the disc perturbations and reconfiguration processes associated with Type II outbursts.

Acknowledgements. This work is based on observations obtained with Swift/BAT and MAXI/GSC. We gratefully acknowledge the teams of both missions for maintaining the instruments, providing high-quality data, and making these data publicly available, which were essential for the completion of this study. This work was supported by the Research Council of Finland Centre of Excellence in Neutron-Star Physics (project 374064). HX acknowledges support from the China Scholarship Council (CSC). LJ acknowledges support from the National Natural Science Foundation of China under grant Nos. 12173103 and 12261141691.

References

Barthelmy, S. D., Barbier, L. M., Cummings, J. R., et al. 2005, Space Sci. Rev., 120, 143
Baykal, A., Kızıloğlu, Ü., Kızıloğlu, N., Beklen, E., & Özbey, M. 2008, A&A, 479, 301
Coe, M. J., Bird, A. J., Hill, A. B., et al. 2007, MNRAS, 378, 1427
Fortin, F., García, F., Chaty, S., Chassande-Mottin, E., & Simaz Bunzel, A. 2022, A&A, 665, A31
Fu, W., Lubow, S. H., & Martin, R. G. 2015a, ApJ, 807, 75
Fu, W., Lubow, S. H., & Martin, R. G. 2015b, ApJ, 813, 105
Gehrels, N., Chincarini, G., Giommi, P., et al. 2004, ApJ, 611, 1005
Huang, R.-T., Ji, L., & Yan, J.-Z. 2025, ApJ, 984, 66
König, O., Fürst, F., Kretschmar, P., et al. 2020, A&A, 643, A128
Kretschmar, P., Salazar, E., Laplace, E., et al. 2015, ATel, 6917, 1
Krimm, H. A., Holland, S. T., Corbet, R. H. D., et al. 2013, ApJS, 209, 14
Kuehnel, M., Mueller, S., Kreykenbohm, I., et al. 2012, ATel, 4577, 1
Kühnel, M., Müller, S., Kreykenbohm, I., et al. 2013, A&A, 555, A95
Laplace, E., Mihara, T., Moritani, Y., et al. 2017, A&A, 597, A124
Lee, U., Saio, H., & Osaki, Y. 1991, MNRAS, 250, 432
Martin, R. G., Nixon, C., Armitage, P. J., Lubow, S. H., & Price, D. J. 2014a, ApJ, 790, L34
Martin, R. G., Nixon, C., Lubow, S. H., et al. 2014b, ApJ, 792, L33
Matsuoka, M., Kawasaki, K., Ueno, S., et al. 2009, PASJ, 61, 999
Monageng, I. M., McBride, V. A., Coe, M. J., Steele, I. A., & Reig, P. 2017, MNRAS, 464, 572
Mushtukov, A., & Tsygankov, S. 2024, in Handbook of X-ray and Gamma-ray Astrophysics, eds. C. Bambi, & A. Santangelo (Singapore: Springer), 4105
Nakajima, M., Negoro, H., Mihara, T., et al. 2020, ATel, 13750, 1
Negueruela, I., & Okazaki, A. T. 2001, A&A, 369, 108
Negueruela, I., Reig, P., Coe, M. J., & Fabregat, J. 1998, A&A, 336, 251
Negueruela, I., Okazaki, A. T., Fabregat, J., et al. 2001, A&A, 369, 117
Okazaki, A. T., & Negueruela, I. 2001, A&A, 377, 161
Okazaki, A. T., Hayasaki, K., & Moritani, Y. 2013, PASJ, 65, 41
Porter, J. M., & Rivinius, T. 2003, PASP, 115, 1153
Reig, P. 2011, Ap&SS, 332, 1
Rikame, K., Paul, B., Sharma, R., & Jithesh, V. 2025, MNRAS, 544, 13
Rivinius, T. 2019, in High-mass X-ray Binaries: Illuminating the Passage from Massive Binaries to Merging Compact Objects, eds. L. M. Oskinova, E. Bozzo, T. Bulik, & D. R. Gies, IAU Symp., 346, 105
Sguera, V. 2017, ATel, 10626, 1
Stollberg, M. T., Finger, M. H., Wilson, R. B., et al. 1993, IAU Circ., 5836, 1
Tsygankov, S. S., Mushtukov, A. A., Suleimanov, V. F., et al. 2017, A&A, 608, A17
Wang, W., Tang, Y. M., Tuo, Y. L., et al. 2021, J. High Energy Astrophys., 30, 1
Wilson, R. B., Harmon, B. A., Fishman, G. J., et al. 1994, in The Evolution of X-ray Binariese, eds. S. Holt, C. S. Day, et al. (AIP), AIP Conf. Ser., 308, 451
Wilson, C. A., Finger, M. H., Coe, M. J., Laycock, S., & Fabregat, J. 2002, ApJ, 570, 287
Wilson, C. A., Fabregat, J., & Coburn, W. 2005, ApJ, 620, L99
Wilson, C. A., Finger, M. H., & Camero-Arranz, A. 2008, ApJ, 678, 1263